CHINESE OPTICS LETTERS

Vol. 19, No. 3 | March 2021

Ultranarrow bandwidth Faraday atomic filter approaching natural linewidth based on cold atoms

Wei Zhuang (庄 伟)*, Yang Zhao (赵 阳), Shaokai Wang (王少凯), Zhanjun Fang (方占军), Fang Fang (房 芳), and Tianchu Li (李天初)

National Institute of Metrology, Beijing 100029, China

*Corresponding author: zhuangwei@nim.ac.cn

Received December 15, 2020 | Accepted January 19, 2021 | Posted Online March 3, 2021

An ultranarrow bandwidth Faraday atomic filter is realized based on cold ^{87}Rb atoms. The atomic filter operates at 780 nm on the $5^2S_{1/2}, F = 2$ to $5^2P_{3/2}, F' = 3$ transition with a bandwidth of 7.1(8) MHz, which is approaching the natural linewidth of the transition. The peak transmission achieves 2.6(3)% by the multi-pass probe method. This atomic filter based on cold atoms may find potential applications in self-stabilizing lasers in the future.

Keywords: Faraday effect; atomic filter; cold atoms; Faraday laser.

DOI: 10.3788/COL202119.030201

1. Introduction

Narrow bandwidth optical filters based on the Faraday effect of the atomic medium have been used in a vast array of applications, such as lidar[1–3], free-space communications[4], quantum optics[5], and, recently, self-stabilizing lasers[6–11]. High peak transmission and narrow bandwidth are key factors of Faraday atomic filters, which have been developed for several alkali atoms based on vapor cells, such as Cs[12,13], Rb[14–17], K[18,19], and Na[20]. Ultranarrow bandwidth atomic filters can be realized by the velocity selective pumping method to reduce the Doppler width of thermal atoms[21]. The bandwidth of the atomic filter for the Rb D2 transition line can achieve 25 MHz, which is still much larger than the natural linewidth[22]. Besides, the center frequency of the atomic filter depends on the pumping laser, which has to be locked to atomic transition lines beforehand. Therefore, the self-stabilizing laser or Faraday laser[10] based on the atomic filter depends on the stabilized pumping laser, which is unfavorable for self-stabilizing systems.

The magneto-optical effect of cold atoms has been extensively studied[23–26]. Since atoms have been laser cooled to a sub-Doppler temperature, the bandwidth of the atomic filter based on cold atoms can approach the natural linewidth, which is much narrower than that based on vapor cells. Moreover, the center frequency depends on the atomic transition line itself rather than the pumping laser, since cold atoms are released freely. For the self-stabilizing laser, the atomic filter based on cold atoms should have ultranarrow bandwidth, stable center frequency, and high transmission. In this Letter, we demonstrate a Faraday atomic filter operating on the Rb D2 transition line with a bandwidth of 7.1(8) MHz based on cold atoms, which have been laser cooled to a temperature below the Doppler limit. To achieve higher peak transmission, the multi-pass probe method has been adopted, resulting in a transmission of up to 2.6(3)%.

2. Theory

The Faraday rotation is a well-known type of magneto-optical effect, i.e., the polarization of a linearly polarized probe light will experience rotation when propagating in the atomic medium along a bias magnetic field. The rotation angle can be simply expressed as[22]

$$\theta = \frac{\pi(n_+ - n_-)L}{\lambda}, \tag{1}$$

where n_+ and n_- denote refractive indices of σ_+ and σ_- components of linearly polarized probe light, L is the length of the atomic medium, and λ is the probe light wavelength. The magnetic field induces Zeeman splitting of the atomic energy levels. The rotation angle can be estimated at small magnetic field when $\mu B \ll \Gamma$, i.e.,

$$\theta \approx b\mu B/\Gamma, \tag{2}$$

where μ is the Bohr magneton, B is the magnetic field, Γ is the natural linewidth, and b is the optical thickness of the atomic sample. Therefore, the Faraday rotation effect can be analyzed based on the above expression.

3. Experiment Setup and Results

The experiment setup is shown in a schematic diagram in Fig. 1. A standard magneto-optical trap (MOT) was utilized for cooling ^{87}Rb atoms. The first 780 nm laser (Quantel Eylsa) is used for MOT cooling, whose frequency is locked to the ^{87}Rb D2 transition line by the saturation absorption spectroscopy (SAS) technique. The main output power (1 W) propagates through an acousto-optical modulator (AOM) used for frequency and intensity controlling and then transfers to the physical system through coupler modules and fibers. The second 780 nm laser (Toptica DL Pro) provides repumping light for the MOT, which is also stabilized to SAS and controlled by the AOM. The repumping light (20 mW) is combined with a cooling laser by a polarization beam splitter (PBS) and eventually coupled into the vacuum system. A separate 1560 nm laser (NKT Photonics Koheras) with a linewidth of about 1 kHz is adopted to probe the Faraday rotation effect of cold atoms. The output light is amplified to about 1 W and injected to a periodically poled lithium niobate (PPLN) crystal to produce 780 nm light by second harmonic generation (SHG) with a power of about 10 mW. A portion of the SHG light with a power of about 3 mW is then directed to the modulation transfer spectroscopy (MTS) setup, where the counter-propagating probe and pump beams interact with Rb atoms in a vapor cell. The MTS is applied to stabilize the probe laser frequency without residual modulation. The other portion is coupled to a fiber and transferred to an optical breadboard near the vacuum system, where the probe light is controlled by two AOMs to produce frequency detunings. A neutral density filter (NDF) is used to change the intensity of probe laser, and two polarization-orthogonal Glan–Taylor prisms (GTPs) with an extinction ratio $10^5:1$ are utilized to perform the detection of Faraday rotation when the probe light propagates through cold atoms. A liquid crystal rotator (LCR) is adopted to compensate for polarization variations caused by window plates of the vacuum system.

Cold atoms can be produced in the MOT composed of six cooling and repumping beams and a gradient magnetic field. After about a loading process of 1 s, about 2×10^8 atoms were trapped with a temperature of about 200 μK. In Fig. 2(a), the black circles illustrate the loading process by measurement of fluorescence, which can be used to deduce the atomic number. The red dots represent the transmitted signal of the probe light when polarizations of two GTPs are set in parallel. From the transmission after the absorption of trapped atoms, the optical thickness b can be deduced by $T = \exp(-b)$ with a result of $b = 0.9(1)$. Then, the MOT was switched off, and cold atoms were released. A homogeneous magnetic field created by two coils along the probe direction with a magnitude of about 3 G was turned on after 5 ms. The probe laser pulse with a power of 10 μW and a diameter of about 1 mm is switched on simultaneously, in which case two GTP polarizations are orthogonal. Figure 2(b) shows the transmitted signal of the probe light on the blue dotted line, which represents the Faraday rotation of released cold atoms.

The probe laser frequency was stabilized from the $5^2S_{1/2}$, $F = 2$ to $5^2P_{3/2}$, $F' = 3$ transition by MTS, as shown in the inset of Fig. 3, and can be varied from −10 MHz to 10 MHz relative to the resonant frequency by AOMs before interacting with atoms. Figure 3 shows the rotation signal in black squares varying with the frequency detuning of the probe laser. The error bars are given by 20 cycles of measurements. The maximum rotation angle reaches 26(3) mrad, corresponding to the peak transmission of 2.6(3)% thanks to the multi-pass probe method. The full width at half-maximum (FWHM) of the atomic filter is

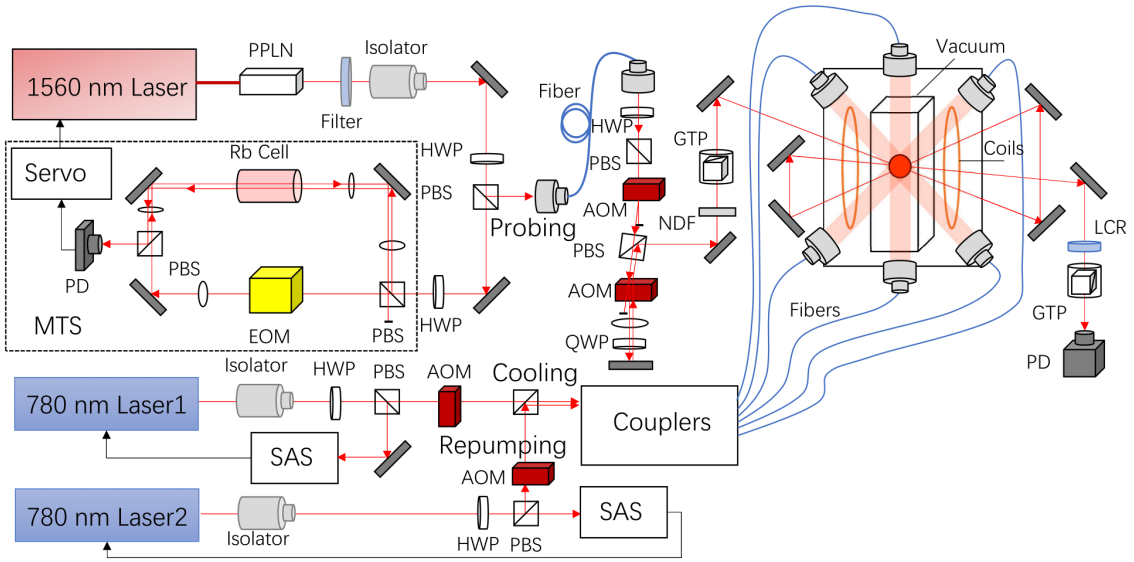

Fig. 1. Schematic diagram of the experiment. PPLN, periodically poled lithium niobate crystal; HWP, half-wave plate; QWP, quarter-wave plate; PBS, polarization beam splitter; PD, photodiode; Servo, servo electronics; EOM, electro-optical modulator; MTS, modulation transfer spectroscopy; SAS, saturation absorption spectroscopy; AOM, acousto-optical modulator; GTP, Glan–Taylor prism; LCR, liquid crystal rotator; NDF, neutral density filter.

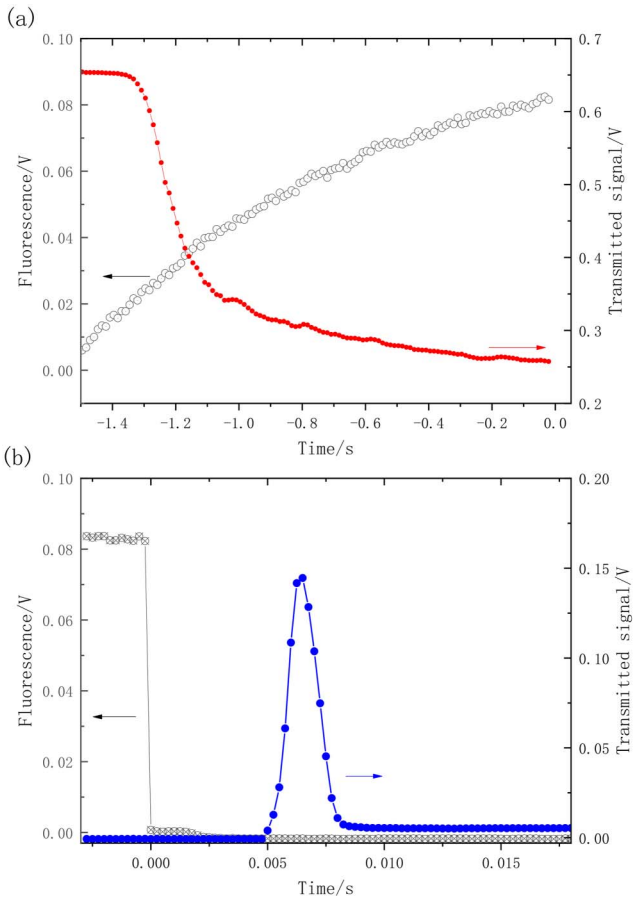

Fig. 2. (a) Fluorescence and absorption signals of trapped cold atoms when GTP polarizations are parallel; (b) fluorescence and transmitted signal of the probe laser due to the Faraday rotation effect of released cold atoms when GTP polarizations are orthogonal. The horizontal axes represent the loading times relative to the time when MOT is shut off.

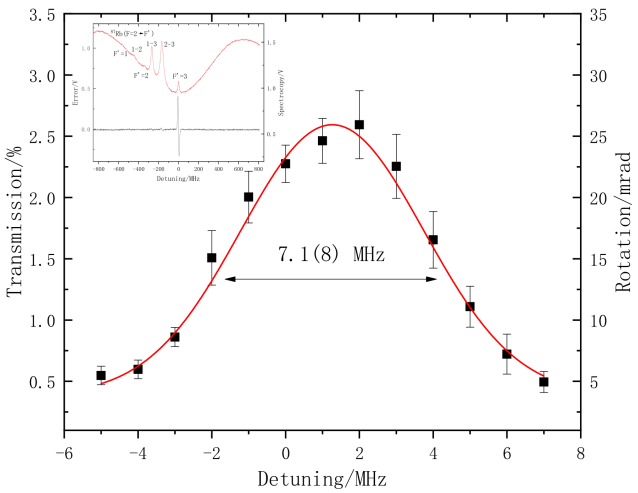

Fig. 3. Transmission spectrum of the Faraday atomic filter. The inset shows the frequency reference for the probe laser.

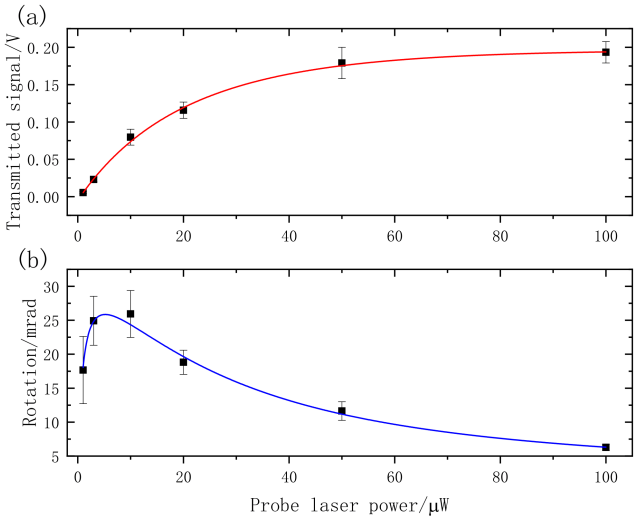

Fig. 4. Dependence of the transmitted signal of probe light and rotation angle on probe laser power with the detuning of 2 MHz. Each data point is an average of 20 measurement results.

evaluated to be 7.1(8) MHz by Gaussian fitting on the red line in Fig. 3. Since the probe laser has a much smaller linewidth, the value represents the actual bandwidth of the atomic filter itself. The center frequency of the filter is slightly blue detuned from the resonant frequency since the probe light would exert a push force to cold atoms and induce the Doppler shift.

The peak transmission of the atomic filter depends on several factors, including atomic number, probe laser power, magnetic field, and so on. To investigate the influence of probe laser power on the peak transmission or the rotation angle, the power was adjusted from 1 μW to 100 μW in the experiment. The transmitted signal of the probe light approaches saturation when increasing the probe laser power, as shown in Fig. 4(a). The rotation angle, which corresponds to the ratio of the transmitted light

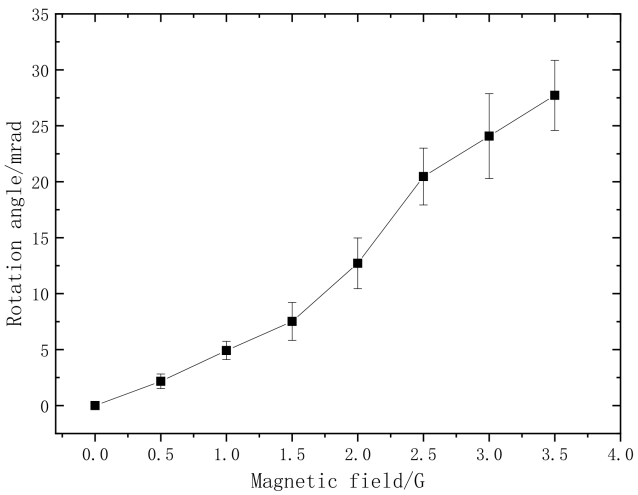

Fig. 5. Rotation angle varies with the applied magnetic field with the probe laser power set at 10 μW and a detuning of 2 MHz. Each data point corresponds to 20 times of measurements.

and the input probe laser, reaches a maximum value due to the saturation effect when the probe laser power is about 5 μW. Therefore, the probe laser power should be set at the appropriate value to obtain a larger rotation angle.

Figure 5 shows the relationship between the rotation angle and the homogeneous magnetic field, which was varied from 0 to 3.5 G by the driving current in coils. The probe laser power is 10 μW, and the frequency is blue detuned 2 MHz relative to the $5^2S_{1/2}, F = 2$ to $5^2P_{3/2}, F' = 3$ transition. The result indicates an approximate linear increase of the rotation angle at small magnetic field values, which coincides with the expression given above.

4. Conclusion

In conclusion, we have demonstrated a Faraday atomic filter based on cold ^{87}Rb atoms released from MOT. The filter is composed of a cold atom sample, two polarization-orthogonal GTPs, and a bias magnetic field. The transmission of the filter reaches a maximum of 2.6(3)%, and the FWHM bandwidth is evaluated to be 7.1(8) MHz, which is approaching the natural linewidth of the $5^2S_{1/2}, F = 2$ to $5^2P_{3/2}, F' = 3$ transition of ^{87}Rb atoms. The relationships between the Faraday rotation angle and probe laser power as well as magnetic field were studied in the experiment. It should be noted that the atomic filter operates in the pulse mode since cold atoms have to be prepared and released before working as a filter. However, if cold atoms are prepared by optical molasses, the atomic filter can be realized in continuous mode, which might be more convenient for applications of optical line filtering and self-stabilizing lasers.

Acknowledgement

This work was supported by the National Natural Science Foundation of China (No. 11704361).

References

1. C. Fricke-Begemann, M. Alpers, and J. Höffner, "Daylight rejection with a new receiver for potassium resonance temperature lidars," Opt. Lett. **27**, 1932 (2002).
2. Q. Qian, Y. Hu, N. Zhao, M. Li, F. Shao, and X. Zhang, "Object tracking method based on joint global and local feature descriptor of 3D LIDAR point cloud," Chin. Opt. Lett. **18**, 061001 (2020).
3. J. Qian, Z. Zheng, M. Lei, C. Song, S. Huang, and X. Gao, "A compact complex-coefficient microwave photonic filter with continuous tunability," Chin. Opt. Lett. **17**, 100601 (2019).
4. J. Tang, Q. Wang, Y. Li, L. Zhang, J. Gan, M. Duan, J. Kong, and L. Zheng, "Experimental study of a model digital space optical communication system with new quantum devices," Appl. Opt. **34**, 2619 (1995).
5. J. S. Neergaard-Nielsen, B. M. Nielsen, H. Takahashi, A. I. Vistnes, and E. S. Polzik, "High purity bright single photon source," Opt. Express **15**, 7940 (2007).
6. X. Miao, L. Yin, W. Zhuang, B. Luo, A. Dang, J. Chen, and H. Guo, "Note: demonstration of an external-cavity diode laser system immune to current and temperature fluctuations," Rev. Sci. Instrum. **82**, 086106 (2011).
7. X. Zhang, Z. Tao, C. Zhu, Y. Hong, W. Zhuang, and J. Chen, "An all-optical locking of a semiconductor laser to the atomic resonance line with 1 MHz accuracy," Opt. Express **21**, 28010 (2013).
8. Z. Tao, Y. Hong, B. Luo, J. Chen, and H. Guo, "Diode laser operating on an atomic transition limited by an isotope ^{87}Rb Faraday filter at 780 nm," Opt. Lett. **40**, 4348 (2015).
9. J. Keaveney, W. J. Hamlyn, C. S. Adams, and I. G. Hughes, "A single-mode external cavity diode laser using an intra-cavity atomic Faraday filter with short-term linewidth < 400 kHz and long-term stability of < 1 MHz," Rev. Sci. Instrum. **87**, 095111 (2016).
10. P. Chang, T. Shi, S. Zhang, H. Shang, D. Pan, and J. Chen, "Faraday laser at Rb 1529 nm transition for optical communication systems," Chin. Opt. Lett. **15**, 121401 (2017).
11. W. Zhuang and J. Chen, "Active Faraday optical frequency standard," Opt. Lett. **39**, 6339 (2014).
12. J. Menders, K. Benson, S. H. Bloom, C. S. Liu, and E. Korevaar, "Ultranarrow line filtering using a Cs Faraday filter at 852 nm," Opt. Lett. **16**, 846 (1991).
13. Y. Wang, S. Zhang, D. Wang, Z. Tao, Y. Hong, and J. Chen, "Nonlinear optical filter with ultranarrow bandwidth approaching the natural linewidth," Opt. Lett. **37**, 4059 (2012).
14. D. J. Dick and T. M. Shay, "Ultrahigh-noise rejection optical filter," Opt. Lett. **16**, 867 (1991).
15. X. Xue, Z. Tao, Q. Sun, Y. Hong, W. Zhuang, B. Luo, J. Chen, and H. Guo, "Faraday anomalous dispersion optical filter with a single transmission peak using a buffer-gas-filled rubidium cell," Opt. Lett. **37**, 2274 (2012).
16. B. Luo, L. Yin, J. Xiong, J. Chen, and H. Guo, "Signal intensity influences on the atomic Faraday filter," Opt. Lett. **43**, 2458 (2018).
17. Z. Tao, M. Chen, Z. Zhou, B. Ye, J. Zeng, and H. Zheng, "Isotope ^{87}Rb Faraday filter with a single transmission peak resonant with atomic transition at 780 nm," Opt. Express **27**, 13142 (2019).
18. B. Yin and T. Shay, "A potassium Faraday anomalous dispersion optical filter," Opt. Commun. **94**, 30 (1992).
19. Y. Zhang, X. Jia, Z. Ma, and Q. Wang, "Potassium Faraday optical filter in line-center operation," Opt. Commun. **194**, 147 (2001).
20. H. Chen, C. Y. She, P. Searcy, and E. Korevaar, "Sodium-vapor dispersive Faraday filter," Opt. Lett. **18**, 1019 (1993).
21. L. D. Turner, V. Karaganov, P. J. O. Teubner, and R. E. Scholten, "Sub-Doppler bandwidth atomic optical filter," Opt. Lett. **27**, 500 (2002).
22. W. Zhuang, Y. Hong, Z. Gao, C. Zhu, and J. Chen, "Ultranarrow bandwidth nonlinear Faraday optical filter at rubidium D2 transition," Chin. Opt. Lett. **12**, 101204 (2014).
23. G. Labeyrie, C. Miniatura, and R. Kaiser, "Large Faraday rotation of resonant light in a cold atomic cloud," Phys. Rev. A **64**, 033402 (2001).
24. J. Nash and F. A. Narducci, "Linear magneto-optic rotation in a cold gas," J. Mod. Opt. **50**, 2667 (2003).
25. B. Zheng, H. Cheng, Y. Meng, L. Xiao, J. Wan, and L. Liu, "Observation of Faraday rotation in cold atoms in an integrating sphere," Chin. Phys. Lett. **31**, 073701 (2014).
26. K. Pandey, C. C. Kwong, M. S. Pramod, and D. Wilkowski, "Linear and nonlinear magneto-optical rotation on the narrow strontium," Phys. Rev. A **93**, 053428 (2016).